Non-Grotthuss Proton Diffusion Mechanism in Tungsten Oxide Dihydrate from First-Principles Calculations

H. Lin, F. Zhou, C. P. Liu, V. Ozolins

October 21, 2013

Disclaimer

This document was prepared as an account of work sponsored by an agency of the United States government. Neither the United States government nor Lawrence Livermore National Security, LLC, nor any of their employees makes any warranty, expressed or implied, or assumes any legal liability or responsibility for the accuracy, completeness, or usefulness of any information, apparatus, product, or process disclosed, or represents that its use would not infringe privately owned rights. Reference herein to any specific commercial product, process, or service by trade name, trademark, manufacturer, or otherwise does not necessarily constitute or imply its endorsement, recommendation, or favoring by the United States government or Lawrence Livermore National Security, LLC. The views and opinions of authors expressed herein do not necessarily state or reflect those of the United States government or Lawrence Livermore National Security, LLC, and shall not be used for advertising or product endorsement purposes.

Proton Diffusion in Tungsten Oxide Dihydrate: Hints from DFT Calculations

Hao Lin,[†] Fei Zhou,[†,‡] Chi-Ping Liu,[†] and Vidvuds Ozoliņš[*,†]

Department of Materials Science and Engineering, University of California, Los Angeles, P.O. Box 951595, Los Angeles, California 90095-1595

E-mail: vidvuds@ucla.edu

Abstract

Knowledge of proton diffusion mechanisms in the tungsten oxide and its hydrates is essential, not only for understanding their conductivity properties but also as fundamental input for designing fuel cell membranes, electrochromics, energy storage materials and gas sensors. It is generally believed that compared with the tungsten oxide and the monohydrate, the tungsten oxide dihydrate is a better proton conductor because of the fast diffusion through its interlayer structural water. Here, we perform density functional theory calculations to test this hypothesis and surprisingly find that proton diffusion mechanisms are similar in the dihydrate and tungsten oxide, and that the interlayer structural water in dihydrate does not directly participated in the fast proton diffusion. Both in the tungsten oxide and the dihydrate, the low activation energy of proton diffusion and the low proton insertion voltage contribute to their relatively high proton conductivity while the high proton activation energy in the monohydrate is responsible for its poor bulk proton conductivity.

---

[*]To whom correspondence should be addressed

[†]Department of Materials Science and Engineering, University of California, Los Angeles, P.O. Box 951595, Los Angeles, California 90095-1595

[‡]Current address: Condensed Matter and Materials Division, Lawrence Livermore National Laboratory, Livermore, California 94550, USA

1 Introduction

Tungsten oxide and its hydrates ($WO_3 \cdot H_2O$ and $WO_3 \cdot 2\,H_2O$) have been widely investigated for their versatile applications in various areas, such as electrochromics, fuel cell membranes, supercapacitor electrodes and gas sensors.[1–7] In the past, tungsten oxide and monohydrate attract more attentions than dihydrate for electrochromic device applications. Recently, tungsten oxide dihydrate ($WO_3 \cdot 2\,H_2O$) was observed to have relatively high proton conductivity (7×10^{-3} S/cm) and low proton activation energy for bulk (0.36 eV) and surface diffusion (0.15 eV),[3] which shows potential as a proton conductor at room temperature. Intuitively, with hydrogen-bonded networks in this structure, proton diffusion should be expected to be a water-mediated process. Additionally, the existence of the interlayer water in tungsten dihydrate, compared to tungsten oxide and monohydrate, is assumed to account for its faster proton conduction. 200 years ago, Grotthuss proposed his revolutionary theory of proton diffusion via the hydrogen-bonded network of water molecules, despite the incorrect chemical formula of water in his discussion.[8] To elaborate the Grotthuss mechanism at atomic scale, Eigen cation, a hydronium core with its three hydrogen atoms hydrogen-bonded to three water molecules, and Zundel cation, a proton equally hydrogen-bonded to two water molecules, were proposed respectively in the years in between 1950s and 1960s.[9–12] Later, *ab initio* molecular dynamics simulations proved that both Eigen and Zundel cations are needed to describe the proton diffusion process in water.[13–15] More recently, Kirchner et al have suggested that hydrogen-bonded networks play an important role in the rapid diffusion of proton in water.[16] Besides in water, hydrogen-bonded networks also have a great influence on proton diffusion in bacteriorhodopsin, a biomolecular machine.[17–19] Furthermore, even without hydrogen-bonded networks, water-mediated process was still found crucial for proton hopping on metal oxide surface.[20]

To our knowledge, despite the intensive investigation of $WO_3 \cdot 2\,H_2O$ by X-ray diffraction, infrared spectrometry, Raman spectroscopy,[3,21–23] no research on proton diffusion in this material has been reported via *ab initio* methods. Here, we investigate the crystal structure, electronic structure, proton intercalations and diffusion properties of tungsten oxide dihydrate by density

functional theory calculations. Interestingly, our result shows that both hydronium and Zundel cation are thermodynamically unstable when an excess proton is introduced in the system. More importantly, it is found that the proton diffuses through the tungsten-oxygen octahedral networks instead of hydrogen-bonded networks in the water layer in this material. Since γ-WO_3 and $WO_3 \cdot H_2O$ have W-O octahedral networks similar to dihydrate, we expect that the proton might diffuse via the W-O octahedral layers as well in these two materials and it is the case in the WO_3. However, this mechanism is not applicable for the monohydrate, and we attribute it as the origins of the various abilities in proton conduction among the $WO_3 \cdot xH_2O$ (x=0,1,2) family.

2 Methodology

Density-functional theory (DFT) calculations were performed to study the structural properties, proton intercalation, electronic structure and proton diffusion of tungsten oxide dihydrate as implemented in the Vienna *Ab initio* Simulation Package (VASP).[24] For all the calculations, we applied the Perdew-Burke-Erzernhof (PBE)[25] exchange correlation functional with the projected augmented wave potentials (PAW).[26] Plane waves with an energy cutoff of 875 eV were used to expand electron wave functions and a $2\times2\times2$ Monkhorst-Pack[27] k-point mesh was used to sample the Brillion zone. Convergence test showed that the total energies with these settings were converged within 2 meV per formula unit, compared to calculations with $10\times10\times10$ Monkhorst-Pack k-point mesh. For all the calculations, the atomic coordinates were fully relaxed until the force on each atom was converged to less than 0.02 eV/Å.

In the dilute limit, the free energies of proton intercalation in the bulk tungsten oxide dihydrate are defined in the following expression:

$$\Delta G^\circ = G[WO_3 \cdot 2H_2O, H] - G[WO_3 \cdot 2H_2O] - \frac{1}{2}G^\circ[H_2] + \Delta E_{zpe} \tag{1}$$

where $G[WO_3 \cdot 2H_2O,H]$ is the total free energy of bulk $WO_3 \cdot 2H_2O$ with an additional hydrogen atom, $G[WO_3 \cdot 2H_2O]$ is the total free energy of bulk $WO_3 \cdot 2H_2O$, $G^\circ[H_2]$ is the free energy

3

of hydrogen gas at 300 K which was discussed in the literature,[28] and ΔE_{zpe}, the zero point energy of the additional hydrogen atom, was found to be 0.293 eV in this system. Using the reversible hydrogen electrode as a reference electrode, we can calculate the voltage of proton insertion at the initial stage in the following:

$$V = \frac{\Delta G^\circ}{e} \tag{2}$$

To investigate the proton diffusion property in tungsten oxide dihydrate, image nudged elastic band (NEB) method[29] was used to find the minimum energy path (MEP) between two local stable sites of proton along possible diffusion paths by interpolating the initial and final states along proton diffusion paths with at least five intermediate images. In addition, the transition state obtained by NEB was further refined using the climbing nudged elastic band (cNEB) method.[30]

3 Results and Discussions

3.1 Structural properties

As shown in Figure 1a, the crystal structure of tungsten oxide dihydrate belongs to the monoclinic $P2_1/n$ space group and its primitive cell contains 16 formula units. The structure framework consists of corner-sharing WO_6 octahedra (grey) (shown in Figure 1b) with two types of water molecules. One type of water molecule ("coordinated water") shares its oxygen with the tungsten ion while the other type of water is interlayer crystal water (See Figures 1a and 1c), which is located within the (010) plane between two layers of WO_6 octahedra. To the best of our knowledge, the crystal structure of $WO_3 \cdot 2\,H_2O$ in the inorganic crystal structure database (ICSD) does not contain the coordinates of hydrogen atoms because the XRD patterns of $WO_3 \cdot 2\,H_2O$ was determined by Cu-Kα radiation (1.54056 Å) which has a larger wavelength than the distance between oxygen and hydrogen.[3] Since $WO_3 \cdot 2\,H_2O$ and $MoO_3 \cdot 2\,H_2O$ share the same space group and exhibit identical atomic arrangements, we relaxed the $WO_3 \cdot 2\,H_2O$ structure by borrowing the hydrogen

positions from the structure of $MoO_3 \cdot 2\,H_2O$ as input. The a, b and c crystal parameters in our first-principles calculation are 10.57 Å, 14.12 Åand 10.67 Å, respectively, slightly larger than the corresponding values in the experiment ($a = 10.48$ Å, $b = 13.97$ Å, $c = 10.62$ Å). The relaxed angle is slightly smaller than that in the experiment. The differences of crystal parameters between our DFT calculation and XRD data are below 3%. These errors can be attributed to the approximate nature of the exchange-correlation functional and have been well understood by the computational chemistry community.[31–33] It is also found that the discrepancy of lattice parameter in the b direction is slightly larger than other two directions. This can be explained by the inappropriate description of the van der Waals force between the interlayer water molecules and WO_6 octahedra in the b direction by the generalized gradient approximation (GGA) in our calculation. To further verify the crystal structure we generated here is able to describe the system properly, we calculated the reaction enthalpy in the dehydration reaction $WO_3 \cdot 2\,H_2O \longrightarrow WO_3 \cdot H_2O + H_2O(l)$. The reaction enthalpy can be defined by:

$$\Delta H = H[WO_3 \cdot H_2O] + H[H_2O] - H[WO_3 \cdot 2\,H_2O] + \Delta_{zpe} \tag{3}$$

where $H[WO_3 \cdot H_2O]$, $H[H_2O]$ and $H[WO_3 \cdot 2\,H_2O]$ are the enthalpies of $WO_3 \cdot H_2O$, H_2O and $WO_3 \cdot 2\,H_2O$ respectively, Δ_{zpe} is the zero point energy corrected term which reduces the error generated by the difference of zero vibrational energy among $WO_3 \cdot H_2O$, H_2O and $WO_3 \cdot 2\,H_2O$. The enthalpies of $WO_3 \cdot H_2O$ and $WO_3 \cdot 2\,H_2O$ can be described appropriately by DFT total energies whereas that of H_2O calculated from DFT directly has large error. Here, we obtained the $H[H_2O]$ by using the reaction enthalpy ΔH_r° (3 kJ/mol) of another dehydration reaction, $WO_3 \cdot H_2O \longrightarrow WO_3 + H_2O(l)$, in the standard condition, and the DFT total energies of $WO_3 \cdot H_2O$ and WO_3:

$$H[H_2O] = E[WO_3 \cdot H_2O] - E[WO_3] + \Delta H_r^\circ - \Delta_{zpe}' \tag{4}$$

where Δ_{zpe}' is the difference of zero point energy between the water and the structural water in the $WO_3 \cdot H_2O$. The reaction enthalpy ΔH in the equation (3) is 36 kJ/mol while in the experiment,

the measured value is 40 kJ/mol, which is an indirectly justification of the validity of our calculation methods.

There are four types of oxygen sites in $WO_3 \cdot 2\,H_2O$ (shown in Figure 1a): coordinated-water oxygen (C-O) in the WO_6 octahedron, bridging oxygen (B-O) in WO_6, terminated-oxygen (T-O) in WO_6, and interlayer-water oxygen (I-O). Within the octahedron, the bonding length between tungsten and terminal oxygen (1.75 Å) is much shorter than that between tungsten and oxygen in the coordinated water molecule (2.31 Å). This difference is due to the stronger bonding between tungsten and T-O than that between tungsten and C-O, as discussed below in Section 3.2 .

With the same space group($P2_1/n$) as dihydrate, the room-temperature monoclinic tungsten oxide(γ-WO_3) is made of the three-dimensional(3D) network of distorted corner-sharing WO_6 octahedra(presented in Figure 2a) while tungsten oxide monohydrate has dihydrate-like layered structure of distorted corner-sharing WO_6 octahedra(see Figure 2b). Compared to the compact 3D structure of γ-WO_3, the hydrates' layered structures are believed to enhance the proton diffusion because of the larger space between the layers as well as the structural water between the layers. The dihydrate is supposed to be even better as a proton conductor than the monohydrate due to its particular interlayer crystal water.

3.2 Electronic structure

As can be seen in Figure 3a, pure tungsten oxide dihydrate exhibits semiconductor behavior with a small band gap in the electronic density of states (DOS). Its energy bands can be divided into three groups of bands: a) the states far below Fermi level between -20 eV and -16 eV mainly originating from the oxygen 2s orbitals, b) the states between -8 eV and 0 eV chiefly coming from the oxygen 2p orbitals, and c) the bands above Fermi level contributed by the tungsten 5d orbitals. In order to reveal the information about the orbital hybridizations in the bond formation, the projected DOS of $WO_3 \cdot 2\,H_2O$ are drawn in Figure 4. Contributed by sp^3 hybridization of the oxygen and hydrogen in the interlayer-water and coordinated-water, valence bands ranging from -20 eV to -19 eV and from -8 eV to -7 eV are lone pairs around the oxygen atoms in the

6

water and σ bonding hybrids of O 2p and H 1s, respectively (see Figure 4). Normally, the d orbitals of metals are expected to be split into three t_{2g} orbitals and two e_g orbitals in an octahedral ligand field. With s and p orbitals in metal, these two e_g orbitals are anticipated to form six hybrid orbitals $e_g^2sp^3$ which form σ bonding with six corresponding ligand sp orbitals.[34] In this case, however, only σ bonding hybrids of bridging/terminated O 2s/2p and W $e_g^2sp^3$ orbitals are observed in the region from -18 eV to -16 eV and from -7 eV to -5 eV, since coordinated-water O 2s orbitals are coupled with coordinated-water H 1s orbitals. As shown in Figure 4, the oxygen ligands form two π-bonds (p_x, p_y) with $e_g^2sp^3$ orbitals in the range between -5 eV and 0 eV, while leaving oxygen p_z orbitals largely nonbonding in the band ranging from -2 eV to -1 eV. These nonbonding oxygen p_z orbitals are mainly from bridging oxygen since $WO_3 \cdot 2\,H_2O$ has the W-O octahedral layer structure in the xy plane. These nonbonding orbitals also explain that proton's preference to the bridging oxygen site is due to the formation of bonding between the proton 1s orbital and nonbonding p_z orbitals in the bridging oxygen(details are discussed in the following paragraph). At the bottom of conduction bands, we observe antibonding hybrids of O 2p and W t_{2g} orbitals followed by antibonding hybrids of O 2s and W $e_g^2sp^3$ orbitals. Based on the discussion above, a molecular orbital scheme for WO_3 is drawn in Figure S1. Comparing the projected DOS among I-O, C-O, B-O, T-O and W-$e_g^2sp^3$, we find that only the bands of B-O and T-O are aligned with that of W-$e_g^2sp^3$. Therefore, I-O and C-O are neglected in the scheme because of their little contribution to the W-O chemical bonds. Notwithstanding the lack of the interlayer water in the $WO_3 \cdot H_2O$, the similarity of crystal structure between the dihydrate and the monohydrate leads to the resemblance in electronic structures between them. They both have similar molecular orbital schemes as well as direct band gaps at the gamma point with 1.16 eV for the dihydrate and 0.85 eV for the monohydrate. Unlike that of γ-WO_3, the electronic structures of these two hydrates do not have dispersion in the direction vertical to the octahedral layer (see Figure S2). The γ-WO_3 also has a direct band gap (1.34 eV). It is well known that density functional theory calculations with generalized gradient approximation underestimate the band gap in the semiconductor and the band gap in the γ-WO_3 can be better described by HSE and GW methods, which give 2.80 eV and

3.26 eV respectively.[35,36] Since the color of both monohydrate and dihydrate samples is yellow,[37] their band gaps also should be expected to be larger than 2 eV.

Then the structures and DOS of proton-intercalated $WO_3 \cdot 2H_2O$ were investigated. Since hydrogen and tungsten exhibit positive charge in this structure, they should not form bonding with each other and we only need to consider the bonding between oxygen and hydrogen. As discussed in the previous section, there are 4 kinds of chemical distinguishable environment of oxygen, which protons are possible to be absorbed to. In order to clarify the most stable proton-intercalated structure, we calculated all the possible proton-intercalated sites. Using a real-space mesh of the primitive cell, these sites were generated by the following criteria: 1) the distance between the extra proton and a oxygen atom is in the range of 0.8 ~ 1.8 Å; 2) the distance between a tungsten atom and the additional proton is larger than 1.2 Å; 3) the distance between a native hydrogen atom and the additional proton is larger than 1.0 Å. Figure 5 shows the free energy of proton intercalation in the $WO_3 \cdot 2H_2O$ versus different sites at 300 K. It was found that protons prefer to be intercalated to the bridging oxygen site, whose lowest free energy is -0.12 eV. In another word, the proton insertion voltage is 0.12 V. If spin orbital effect is included, the voltage is 0.03 V higher.[35] For the other three types of oxygen sites, the free energies are positive, indicating that proton absorption at these oxygen sites is thermodynamically unfavorable at zero voltage. Furthermore, proton on the coordinated-water oxygen site is both thermodynamically unfavorable and kinetically unstable, because it repels the coordinated-water oxygen while relaxing towards and bonding to either terminated oxygen or interlayer-water oxygen. The spread of energies for each type of oxygen site in Figure 5 is due to the intrinsic distortion of WO_6 octahedra and the various orientations of two types of water near the intercalation sites in this system.

We took the proton-intercalated structure with lowest total energy for the further electronic structure analysis. When introduced a hydrogen atom into the system, tungsten oxide dihydrate becomes metallic (see Figure 3b). Compared to the electronic density of states of pure $WO_3 \cdot 2H_2O$, the DOS in proton-intercalated $WO_3 \cdot 2H_2O$ does not change much, except for the shift of the Fermi level from the original forbidden band to the conduction band minimum where empty

W 5*d* orbitals originally locate. Interestingly, we find the two-dimensional metallic behavior of proton-intercalated $WO_3 \cdot 2H_2O$ by visualizing the charge density distribution of the extra electron (shown in Figure 6). It can be seen that this electron is largely confined around the O-H group with small delocalization into W $5d_{xz}$ orbitals around the same tungsten layer. We cannot see this extra electron charge density in another tungsten layer because of the isolation by the water molecule network between the tungsten layers. This is consistent with our electronic band calculations, which show that there is no dispersion in the direction perpendicular to the water layer (shown in Figure S2).

3.3 Proton diffusion in tungsten oxide dihydrate

To investigate the activation barrier of proton diffusion, we used nudged elastic band method to find the minimum energy path and applied the climbing image nudged elastic band method to correct the activation energy. In addition, the activation barriers at 300 K were further modified by considering the quantum tunneling effects.[38]

In the water or materials with hydrogen-bonded networks, the proton usually diffuses via the water networks. In this process, at first hydronium is formed, with a hydrogen atom approaching to a water molecule. Then the interaction between one of the hydrogen in the hydronium and another water molecule leads to the formation of Zundel cation ($[H_2O \cdots H \cdots OH_2]^+$), which is believed to be the transition state in the diffusion. After that, one of the hydrogen in the Zundel cation jumps to the nearest water molecule and finish the hopping process.[39] Here, however, we observe an unexpected proton diffusion phenomenon in the material with hydrogen-bonded networks. As indicated in the red arrow, Figure 7a presents a one-dimensional proton diffusion path through the tungsten oxygen octahedral layers. Nevertheless, this one-dimensional proton diffusion path leads to a two dimensional diffusion process because of the symmetry of the octahedral layer. Rather than hopping to the neighbor oxygen site in the hole between octahedra, proton prefers jumping in the diagonal directions in the hole through the W-O layers, because of the lower activation energy in the diagonal directions as plotted in Figure 7b. For the hopping process between the

9

neighbor oxygen sites, the large distortion of octahedron in the transition state contributes to the higher activation energy (see supporting materials, Movie S1). As shown in Figures 7c and 7d, the diagonal diffusion process consists of two distinguishable events. At the beginning of this process, a proton prefers a site near the bridging oxygen in the W-O octahedron. Then the proton rotates about 180 degrees about the W-O-W axis linking two octahedra (rotation around O4, step 1) and hops towards the diagonal bridging oxygen (O4→O7, step 2). After the hopping, the proton rotates again which is the same as step 1. The activation energy of this process is 0.42 eV, which is consistent with the value (0.36 eV) of experimental observations.[3] The small energy barrier difference between O1→O4 and O4→O7 is caused by the different arrangement of coordinated-water in the octahedra. Interestingly, the cost of proton rotation around the W-O-W axis is low even though it leads to the rotations of the neighbor octahedra around the b axis (see supporting materials, Movie S1). To examine the strain caused by these octahedral rotations can be relaxed in a considerable small region, a $\sqrt{2} \times 1 \times \sqrt{2}$ supercell was built to calculate the activation barrier of proton rotations (see supporting materials, Movie S2). The proton rotation activation barrier in this supercell is 215 meV, which is consistent with the values obtained from the primitive cell. Counter-intuitively, the structural water is not involved in the proton diffusion process directly. In another word, the Zundel mechanism is not favored here. The reasons for this phenomenon are in the following: 1) In spite of two types of structural water in the dihydrate, the coordinated water is not able to form a Zundel cation with the other coordinated water and interlayer water because the C-O, one of the ligands in the WO_6 octahedra, always points toward the tungsten atom with hydrogen atoms in the coordinated water far from the tungsten atom. 2) The nearest distance between two I-O atoms is 3.55 Å, while usually the formation of a $H_5O_2^+$ requires much closer oxygen-oxygen distance (2.6~2.8 Å).[40]

Since a proton diffuses through the octahedral layer in the dihydrate without the direct assistance of the structural water, similar proton diffusion mechanisms should be anticipated in γ-WO_3 and $WO_3 \cdot H_2O$. As expected, we find that the proton diffusion in the γ-WO_3 also follows the same two-step process as that in the dihydrate. Our calculated proton activation energy here is 0.35 eV,

while Randin et al gave a value of 0.4 eV in their measurement.[41] The predicted proton insertion voltage in γ-WO_3 is 0.11 V, which reproduces the redox peak position(0.2 V relative to SHE) in the cyclic voltammetry measurement with the sweep rate of 3.5 mV/s in the literature.[1] These two main characters largely guarantee the tungsten oxide and its dihydrate being practical proton conductors for electromic devices and other proton conducting applications. For the monohydrate, however, our DFT results indicate that the absorption energy of the extra proton to the terminated oxygen site is 0.2 eV lower than that to the bridging oxygen site, suggesting that the alien proton prefers to the terminated oxygen site in it. The voltage of the proton intercalation to the T-O site in the bulk is 0.97 V in our calculation whereas in experiment the position of redox peak in the cyclic voltammetry measurement during the discharge is 0.35 V. The discrepancy here is unclear but experimental observations indicated that proton diffusion in monohydrate must be a surface process and surface oxygen vacancies are likely to be involved in such process.[3,42] We suggest that this redox peak in the experiment might only reflect the surface insertion properties instead of bulk insertion properties. Even if assuming the high proton insertion voltage would not be a problem, the high proton diffusion barrier in the monohydrate still hinders its potential for proton conducting applications. The proton diffusion in the (010) plane between the octahedral layer proves difficult in our calculations due to the high activation barrier (?? eV). Admittedly, proton diffusion activation energy through the W-O octahedral layers is comparable to that in the γ-WO_3 and the dihydrate, if proton's absorbing to the bridging oxygen site is treated as the starting point. The problem is that the barrier of proton's jumping from the T-O site to the B-O site is ??? eV, suggesting that the diffusion path through the octahedral layers is unfavorable.

4 Conclusion

In summary, demonstration of proton diffusion mechanisms among the $WO_3 \cdot xH_2O$ (x=0,1,2) family has been presented. We have analyzed the crystal structure, electronic structure,proton-intercalated structures and proton diffusion in the tungsten oxide dihydrate. The proton has been

11

found to be energetically favorable to intercalate in the tungsten octahedral layers, forming chemical bonds with bridging oxygen. The proton diffusion activation barrier obtained by transition state theory is 0.42 eV, which is consistent with the experimental result. Revealing that proton diffusion is without the direct assistance of the structure water in this system, we surprisingly find that proton diffusion mechanisms in $WO_3 \cdot 2\,H_2O$ and γ-WO_3 are the same. For the $WO_3 \cdot H_2O$, due to the lack of proton diffusion paths in the bulk structure, it is not a practical proton conductor. Beyond tungsten oxide dihydrate, our investigation may facilitate the understanding of proton diffusion in other metal oxide hydrates.

Acknowledgement

References

(1) Di Paola, A.; Di Quarto, F.; Sunseri, C. *Journal of The Electrochemical Society* **1978**, *125*, 1344–1347.

(2) Xie, Z.; Gao, L.; Liang, B.; Wang, X.; Chen, G.; Liu, Z.; Chao, J.; Chen, D.; Shen, G. *Journal of Materials Chemistry* **2012**, *22*, 19904–19910.

(3) Li, Y.; Hibino, M.; Miyayania, M.; Kudo, T. *Solid State Ionics* **2000**, *134*, 271–279.

(4) Tanaka, Y.; Miyayama, M.; Hibino, M.; Kudo, T. *Solid state ionics* **2004**, *171*, 33–39.

(5) Yoon, S.; Kang, E.; Kim, J. K.; Lee, C. W.; Lee, J. *Chemical Communications* **2011**, *47*, 1021–1023.

(6) Zou, B.-X.; Liang, Y.; Liu, X.-X.; Diamond, D.; Lau, K.-T. *Journal of Power Sources* **2011**, *196*, 4842–4848.

(7) Sekimoto, S.; Nakagawa, H.; Okazaki, S.; Fukuda, K.; Asakura, S.; Shigemori, T.; Takahashi, S. *Sensors and Actuators B: Chemical* **2000**, *66*, 142–145.

(8) de Grotthius, C. *The Philosophical Magazine: Comprehending the Various Branches of Science, the Liberal and Fine Arts, Agriculture, Manufactures and Commerce* **1806**, *25*, 330–339.

(9) Wicke, E.; Eigen, M.; Ackermann, T. *Zeitschrift für Physikalische Chemie* **1954**, *1*, 340–364.

(10) Eigen, M. *Angewandte Chemie* **1963**, *75*, 489–508.

(11) Eigen, M. *Angewandte Chemie International Edition in English* **1964**, *3*, 1–19.

(12) Zundel, G.; Metzger, H. *Zeitschrift für Physikalische Chemie* **1968**, *58*, 225–245.

(13) Tuckerman, M. E.; Laasonen, K.; Sprik, M.; Parrinello, M. *Journal of Physics: Condensed Matter* **1994**, *6*, A93.

(14) Tuckerman, M.; Laasonen, K.; Sprik, M.; Parrinello, M. *The Journal of chemical physics* **1995**, *103*, 150.

(15) Tuckerman, M.; Laasonen, K.; Sprik, M.; Parrinello, M. *The Journal of Physical Chemistry* **1995**, *99*, 5749–5752.

(16) Kirchner, B.; Stubbs, J.; Marx, D. *Physical review letters* **2002**, *89*, 215901.

(17) Spassov, V. Z.; Luecke, H.; Gerwert, K.; Bashford, D. *Journal of molecular biology* **2001**, *312*, 203–219.

(18) Garczarek, F.; Brown, L. S.; Lanyi, J. K.; Gerwert, K. *Proceedings of the National Academy of Sciences of the United States of America* **2005**, *102*, 3633–3638.

(19) Garczarek, F.; Gerwert, K. *Nature* **2005**, *439*, 109–112.

(20) Merte, L. R.; Peng, G.; Bechstein, R.; Rieboldt, F.; Farberow, C. A.; Grabow, L. C.; Kudernatsch, W.; Wendt, S.; Lægsgaard, E.; Mavrikakis, M.; Besenbacher, F. *Science* **2012**, *336*, 889–893.

(21) Choi, Y.-G.; Sakai, G.; Shimanoe, K.; Miura, N.; Yamazoe, N. *Sensors and Actuators B: Chemical* **2002**, *87*, 63–72.

(22) Balázsi, C. *Materials Structure* **1999**, *6*, 135.

(23) Daniel, M.; Desbat, B.; Lassegues, J.; Gerand, B.; Figlarz, M. *Journal of solid state chemistry* **1987**, *67*, 235–247.

(24) Kresse, G.; Furthmüller, J. *Computational Materials Science* **1996**, *6*, 15–50.

(25) Perdew, J. P.; Burke, K.; Ernzerhof, M. *Physical review letters* **1996**, *77*, 3865.

(26) Blöchl, P. E. *Physical Review B* **1994**, *50*, 17953.

(27) Monkhorst, H. J.; Pack, J. D. *Physical Review B* **1976**, *13*, 5188–5192.

(28) Ozolins, V.; Zhou, F.; Asta, M. *Accounts of chemical research* **2013**, *46*, 1084–1093.

(29) Jonsson, H.; Mills, G.; Jacobsen, K. W. **1998**,

(30) Henkelman, G.; Uberuaga, B. P.; Jónsson, H. *The Journal of Chemical Physics* **2000**, *113*, 9901.

(31) Fuchs, M.; Bockstedte, M.; Pehlke, E.; Scheffler, M. *Physical Review B* **1998**, *57*, 2134.

(32) Fuchs, M.; Da Silva, J.; Stampfl, C.; Neugebauer, J.; Scheffler, M. *Physical Review B* **2002**, *65*, 245212.

(33) Fischer, C. C.; Tibbetts, K. J.; Morgan, D.; Ceder, G. *Nature materials* **2006**, *5*, 641–646.

(34) Sorantin, P. I.; Schwarz, K. *Inorganic Chemistry* **1992**, *31*, 567–576.

(35) Ping, Y.; Rocca, D.; Galli, G. *Physical Review B* **2013**, *87*, 165203.

(36) Wang, F.; Di Valentin, C.; Pacchioni, G. *The Journal of Physical Chemistry C* **2011**, *115*, 8345–8353.

(37) Freedman, M. L. *Journal of the American Chemical Society* **1959**, *81*, 3834–3839.

(38) Fermann, J. T.; Auerbach, S. *The Journal of Chemical Physics* **2000**, *112*, 6787.

(39) Marx, D. *ChemPhysChem* **2006**, *7*, 1848–1870.

(40) Muguet, F. F. *Journal of Molecular Structure: THEOCHEM* **1996**, *368*, 173–196.

(41) Randin, J.-P.; Viennet, R. *Journal of The Electrochemical Society* **1982**, *129*, 2349–2354.

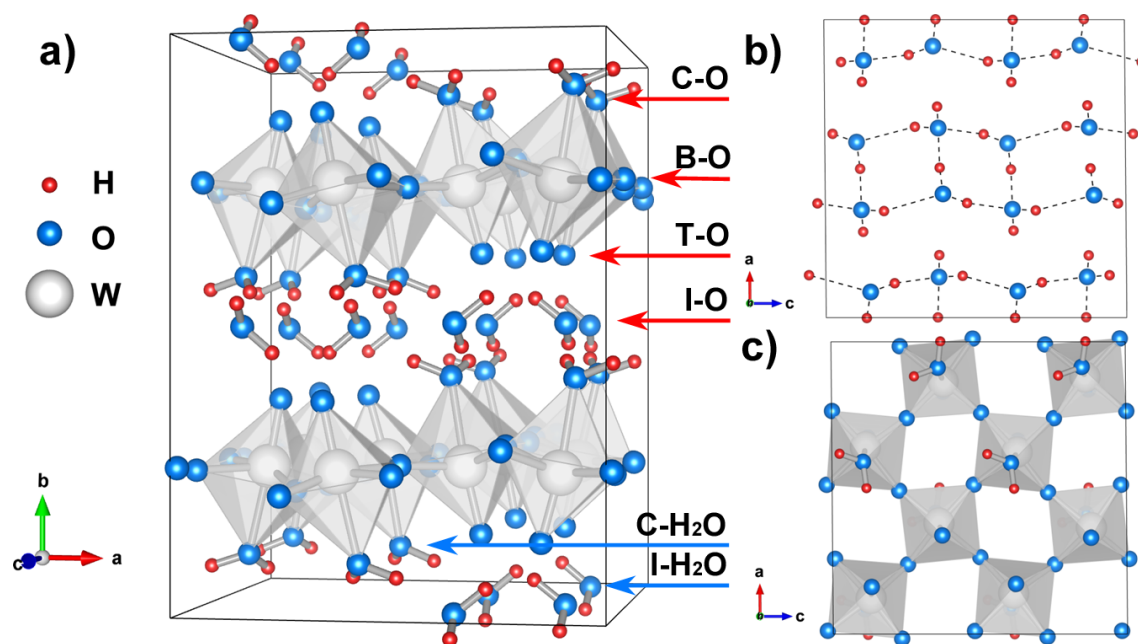(42) Randin, J. *Journal of Electronic Materials* **1978**, *7*, 47–63.

Figure 1: a) Crystal structure of tungsten oxide dihydrate, where C-O, B-O, T-O and I-O represent coordinated-water oxygen, bridging oxygen, terminated-oxygen and interlayer-water oxygen respectively, and C-H$_2$O, I-H$_2$O denote coordinated water and interlayer water, b) a tungsten-oxygen octahedral layer, c) hydrogen-bonded network.
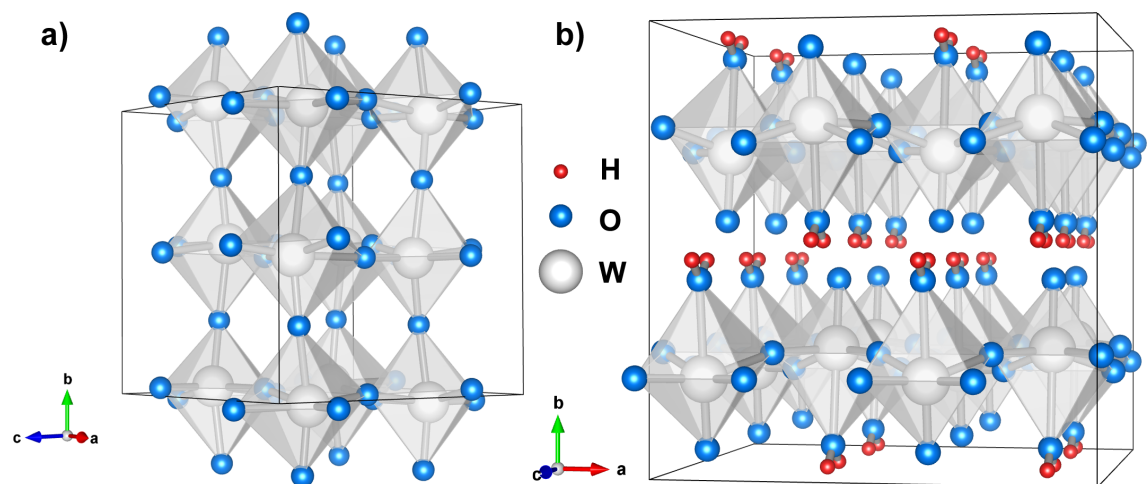
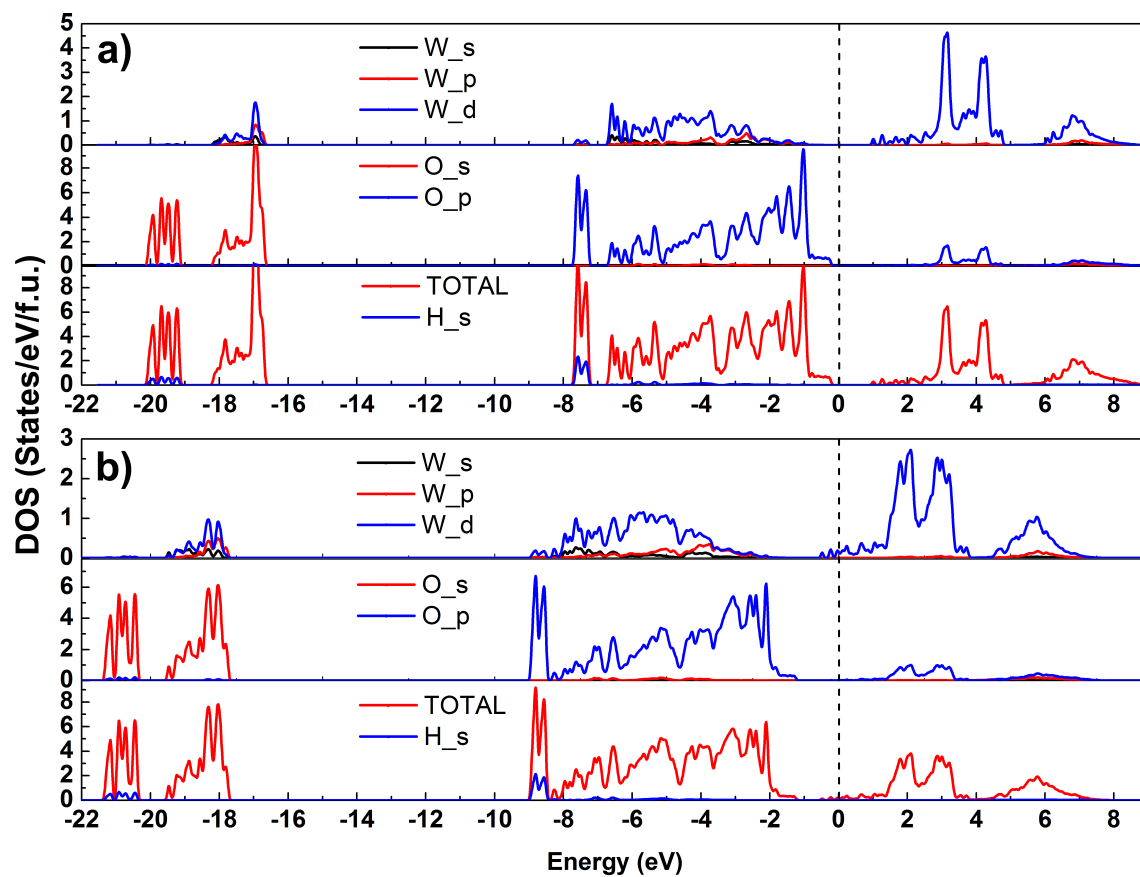Figure 2: Crystal structure of a)the room-temperature tungsten oxide(γ-WO₃) and b) the tungsten oxygen monohydrate.

Figure 3: Electronic density of states for a) pure tungsten oxide dihydrate, b) proton-intercalated tungsten oxide dihydrate; Fermi level was set to zero.
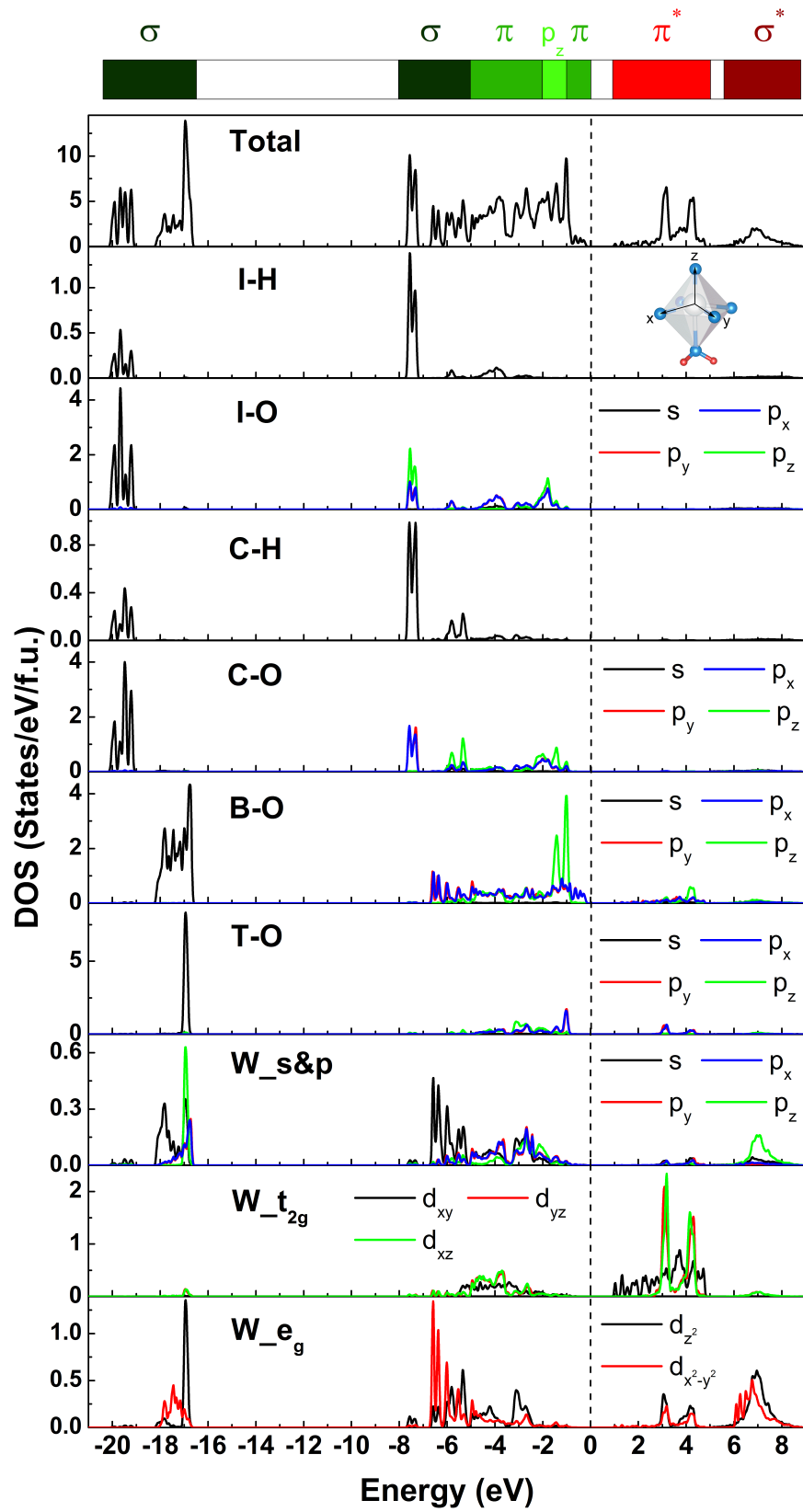
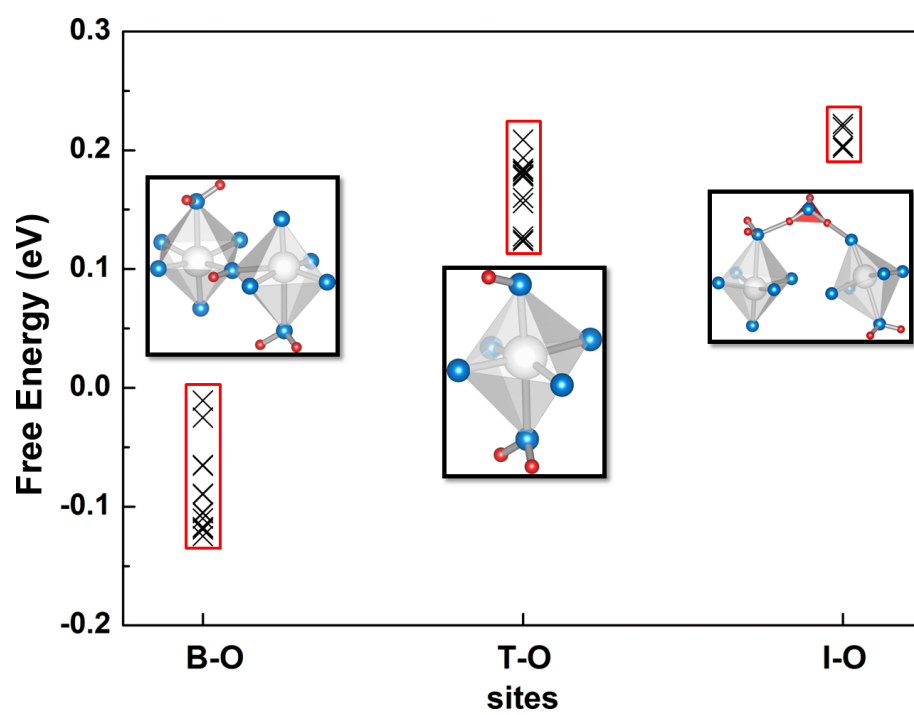Figure 4: Projected electronic density of states for pure $WO_3 \cdot 2\,H_2O$. Fermi level was set to zero.
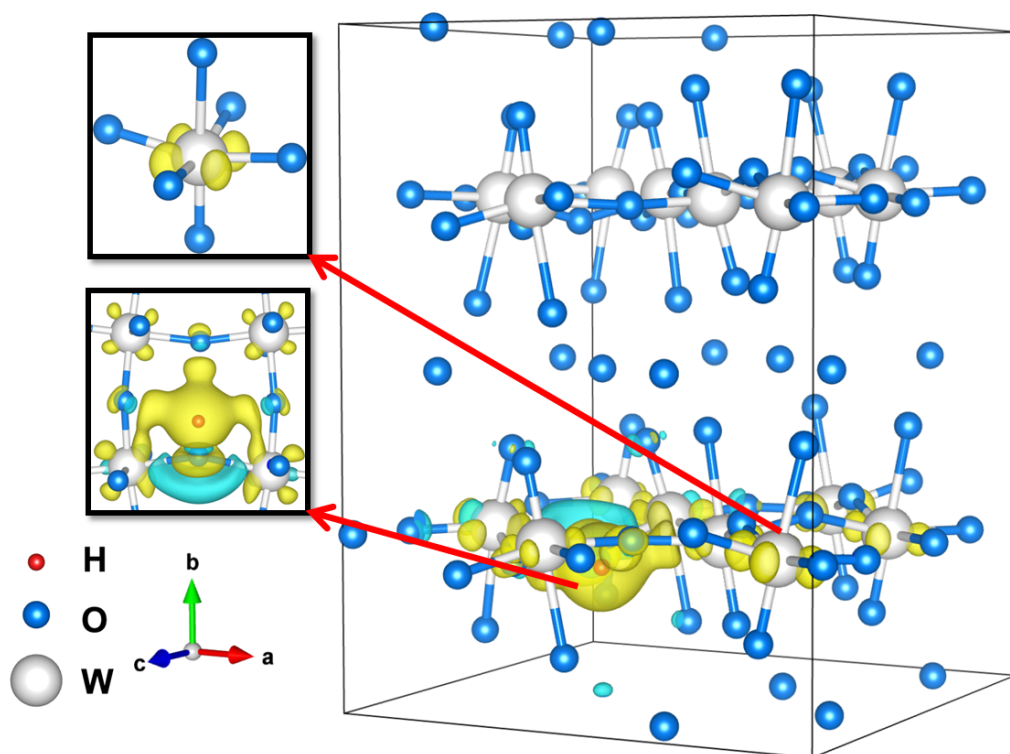
Figure 5: Free energy of proton intercalation in the $WO_3 \cdot 2\,H_2O$.

Figure 6: Charge density distribution of an additional electron in proton-intercalated $WO_3 \cdot 2\,H_2O$ relative to $WO_3 \cdot 2\,H_2O$. To facilitate the comparison, the atoms in $WO_3 \cdot 2\,H_2O$ are fixed to their positions in proton-intercalated $WO_3 \cdot 2\,H_2O$. Hydrogen atoms are not shown here except the extra hydrogen atom (red). The electron accumulation region is shown in yellow while the depletion region drawn in green.
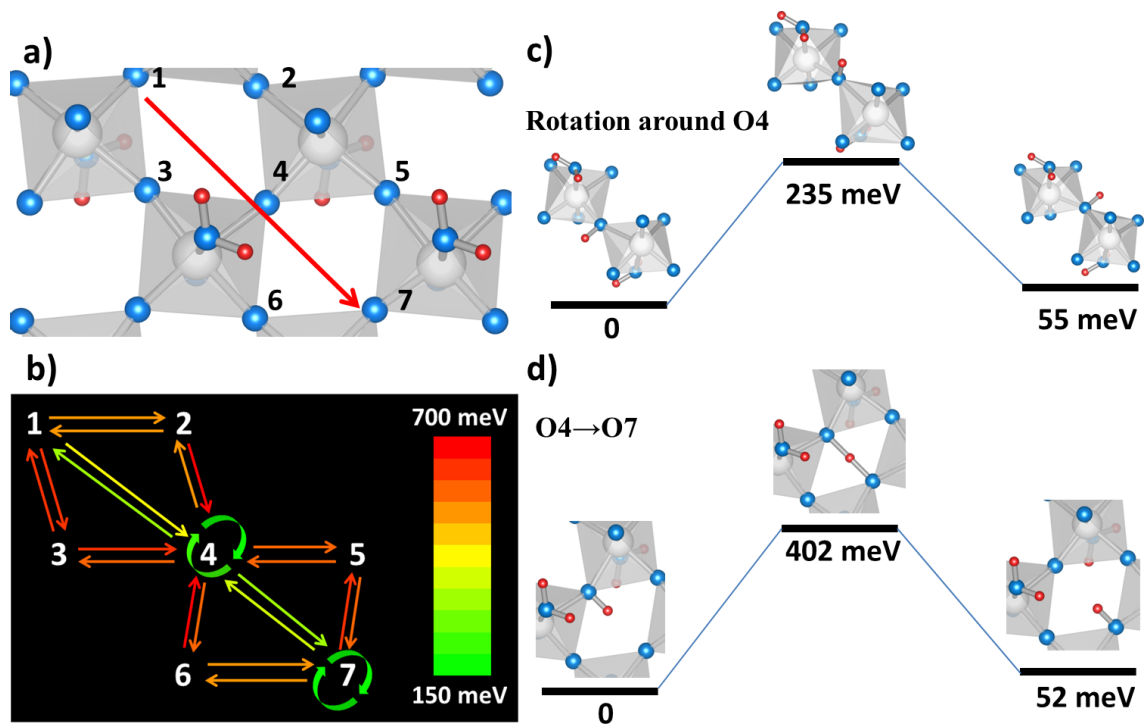
Figure 7: a) proton diffusion path; b) indicates the activation barriers of proton diffusion; transition states of c) proton rotation around O4 and d) proton hopping from O4 to O7.